Formulation of a truss element for modelling the tensile response of FRCM strips

Giovanni Minafò[a,*], Maria Concetta Oddo[a], Lidia La Mendola[a]

[a] *Università degli Studi di Palermo, Dipartimento di Ingegneria, Viale delle Scienze Ed.8, 90128 Palermo, Italy*

Abstract

Modelling the tensile behaviour of Fabric Reinforced Cementitious Matrix (FRCM) is not a straightforward task due to the inner complexity of the mechanics of this kind of composite materials. In fact, after that the matrix is cracked, the compatibility between the fiber and the surrounding mortar is lost and the system behaves as two separate elements connected by a brittle interface. For this reason, several research studies proposed computational approaches for evaluating the tensile behaviour of FRCM composites, usually referring to brick-based 3D Finite Element Models (FEM) or to complex numerical procedures. This paper shows the formulation of a simplified coupled truss element for modelling the tensile behaviour of FRCM composites. The proposed element includes the interface slip between fiber and matrix and the brittle failure of the fabric and allows to describe the response of the system between the cracks in closed form. The proposed element is also adopted for assessing the tensile constitutive response of FRCMs through a simplified assembly procedure, proving to be reliable and computationally efficient.

Keywords: FRCM, tensile behaviour, cracking, interface

*Corresponding author
Email address: giovanni.minafo@unipa.it (Giovanni Minafò)

1. Introduction

The use of Fabric Reinforced Cementitious Matrix (FRCM) composites has become increasingly popular for applications in masonry structures in the last ten years [1]. Its popularity depends especially from the advantages arising from their applications when applied on masonry surfaces of historical buildings, especially due to the good compatibility between the inorganic matrix and the masonry substrate. For this reason, a huge amount of research works was recently carried out for characterizing the constitutive behaviour of these materials, with particular reference to the tensile behaviour and the bond with masonry [2][3].

The tensile behaviour of FRCM composites proved to be complex and affected from the interaction between matrix and fabric. In fact, after that matrix is cracked, the compatibility between fiber and mortar is lost and the fabric tends to slip with respect to the surrounding mortar. Failure can be reached due to the tensile breakage of the fiber yarns or due to the de-bonding at the the fabric-matrix interface.

The experimental studies available in the recent literature and concerning the mechanical characterization of FRCM composites highlighted a wide variability of results due to the great number of variables involved, including the nature of the fiber, matrix grade, test set-up, the treatment of the fabric surface. As a consequence, a huge amount of research work has been carried out in the last years, investigating on the effect of the different key parameters. Numerous studies were performed on the kind of fibre, such as basalt [4] [5] [6] [7] [8], carbon [9] [10] [11], glass [9] [12] and Polybenzoxazole (PBO) [13] [14]. Other studies investigated the role of the test set-up, analyzing the role of the boundary loading conditions, such as the clevis or clamping grip [15] [16] or the capabilities of the Digital Image Correlation (DIC) for providing more detailed data on the field of strains or displacements [2] [8].

In this background, despite several experimental studies were performed on this topic, fewer studies addressed analytical or numerical approaches for modelling the tensile behaviour of FRCM strips. Simplified analytical models were proposed in the past [4] [17], aiming to model the behaviour of the composite with a multilinear shape, following the well-known rules adopted for reinforced concrete members. Other works followed a numerical approach, often based on 3D Finite Element (FE) models. In this context a FE multiscale approach was proposed by Bertolesi et al. [13] for modelling the bond behaviour with the substrate, while Monaco et al. [18] [19] modelled the tensile behaviour of FRCM by adopting a cohesive interface between matrix and fabric. Both works adopted the Concrete Damage Plasticity model for simulating the tensile behaviour of the matrix and assumed a bilinear law with damage for the interface. More recently, a simplified uniaxial model was proposed by Grande and Milani [20], who also proposed recently [21] numerical strategies to solve the governing equations of uniaxial models of FRCM strips under different loading conditions.

Despite these numerical approaches provide a detailed mechanical response of the FRCM systems, they require a complex calibration of the model for assessing the input variables, which are often unknown and should be empirically or tentatively estimated, with the risk of including unavoidable uncertainties. Additionally, the 3D brick-based FE simulations require a strong computational cost, including long calculation time and numerical convergence issues, such as mesh sensitivity, hourglassing or locking.

In this context, this paper presents a novel formulation of a coupled truss element for calculating the tensile response of FRCM strips. The governing equation of the element is obtained in strong form by analyzing the force transmission mechanism between fabric and matrix within the crack spacing. The two phases are modeled as two truss elements connected by a pure shear interface, under the assumption of brittle linear behaviour of materials and interface. Previous studies [22] [23] highlighted that the load transfer mechanism in FRCM composites is more complex than only shear stress transfer at the fabric to matrix interface. The textile of the FRCM systems is multidirectional, generally bidirectional, fabric and the mortar-textile interlock at the voids of fabric known to be one of the stress-transfer mechanisms. However, the proposed paper aims to provide a simple model for achieving the local and global response, respecting a phenomenological/empirical formulation of the interface, which respects the experimental observation. The formulation allows to achieve the local response within the crack spacing in terms of elongations, internal forces and shear stress at the interface. The proposed element is therefore adopted for assembling a procedure for calculating the tensile response of FRCM strips. Results are finally compared with experimental results available in the literature, showing good agreement. The proposed procedure keeps the accuracy of a formulation capable of obtaining the local and global response of the composite material but with the advantage of reducing the computational cost with respect to brick-based 3D FEM analyses. Additionally, it requires the calibration of only one mechanical parameter i.e. the shear stiffness of the interface k , which is here proposed as a function of the mechanical properties of the fabric and of the number of textile layers adopted.

2. Element formulation

The proposed formulation is based on the study of a part of FRCM strip between two successive cracks with length equal to s (Figure 1). It is assumed that the behaviour of the composite between the cracks can be represented by two sub-elements, represented by the matrix and the fabric, each one with truss behaviour and with axial stiffness equal to $E_m A_m$ and $E_f A_f$ respectively, as shown in Figure 1. The two elements are connected by a continuous shear interface, with stiffness k ,for sake of simplicity the interactions with transverse bundles of bidirectional textile are neglected, according to experimental

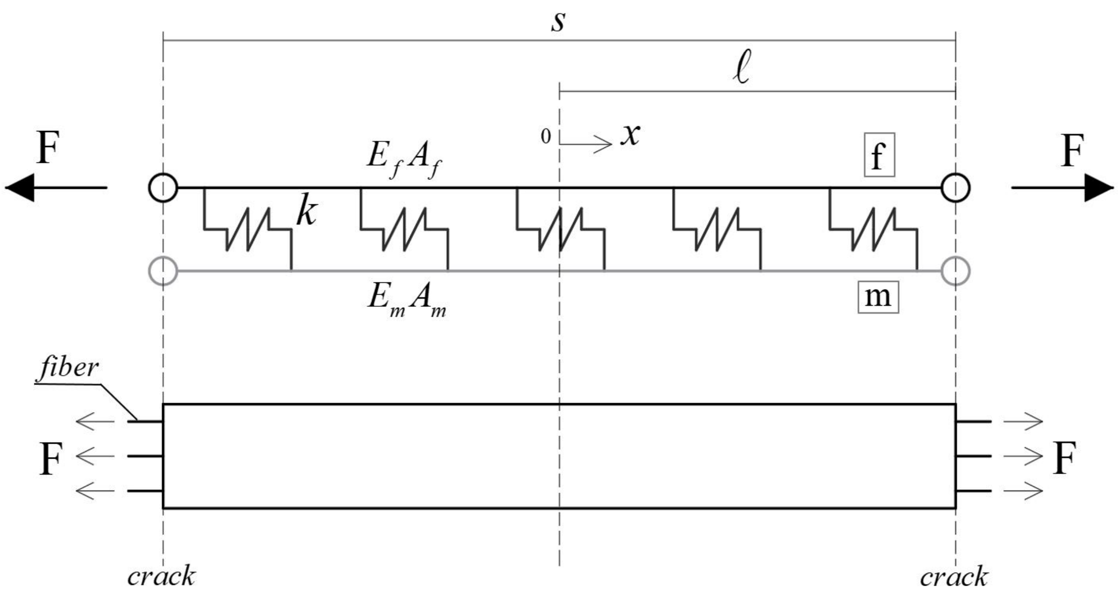

Figure 1: Coupled truss model

evidence [9]. All the materials are assumed to be elastic with a pure brittle constitutive law. The axial elongations of the fiber and matrix are denoted as $u_f(x)$ and $u_m(x)$.

Under the assumptions of Figure 2, the equilibrium equation of the mortar layer can be written as

$$\frac{d^2 u_m(x)}{dx^2} = \frac{p_x(x)}{E_m A_m} \tag{1}$$

being $p_x(x)$ the shear force per unit length transferred from the fiber through the interface.

The constitutive law of the interface is assumed to be elastic with pure brittle behaviour, which means that a linear relation can be established between the shear stress and the relative axial elongation of the elements. In this way, the shear stress per unit length is expressed as

$$p_x(x) = \tau(x) t_i = k(u_f(x) - u_m(x)) t_i \tag{2}$$

where t_i is the depth of the interface. If Eq.2 is assumed, the equilibrium equation of the

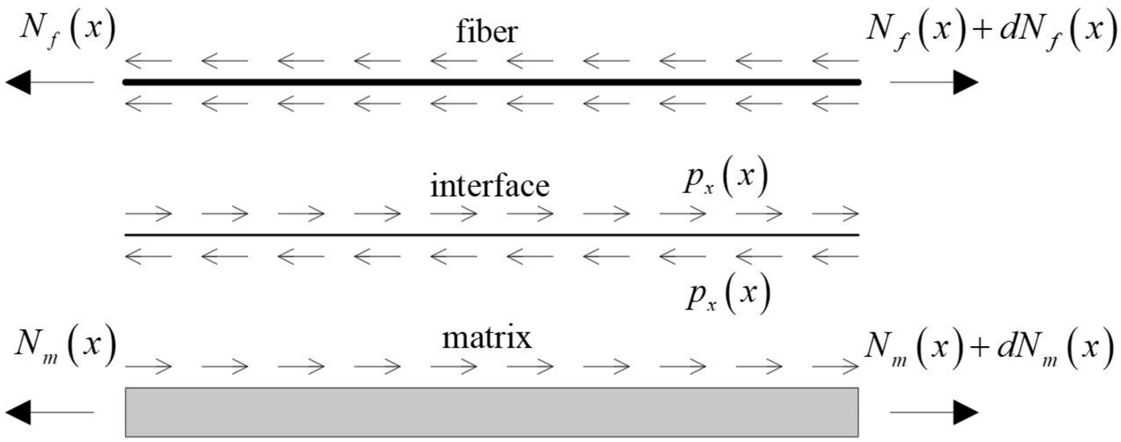

Figure 2: Internal forces and sign assumptions

matrix is written as

$$\frac{d^2u_m(x)}{dx^2} = -\frac{k}{E_mA_m}(u_f(x) - u_m(x))t_i \tag{3}$$

The equilibrium of the fabric can be expressed with similar considerations, leading to the following differential form of the equilibrium

$$\frac{d^2u_f(x)}{dx^2} = \frac{k}{E_fA_f}(u_f(x) - u_m(x))t_i \tag{4}$$

Eqs.3 and 4 represent a system of two ordinary differential equations for calculating the axial response of the system in terms of $u_f(x)$ and $u_m(x)$. A convenient expression of this system can be written in the following form

$$\frac{d^2u_m(x)}{dx^2} + \beta_m^2(u_f(x) - u_m(x)) = 0 \tag{5a}$$
$$\frac{d^2u_f(x)}{dx^2} - \beta_f^2(u_f(x) - u_m(x)) = 0 \tag{5b}$$

where β_m and β_f are the two relative stiffness parameters between the mortar or the fabric and the interface

$$\beta_m = \sqrt{\frac{kt_i}{E_m A_m}} \tag{6a}$$

$$\beta_f = \sqrt{\frac{kt_i}{E_f A_f}} \tag{6b}$$

and observing that from a dimensional point of view both parameters are the inverse of a length.

The two equations of the system can be coupled together by considering the relation between the functions $u_m(x)$ and $u_f(x)$ from Eq.5a

$$u_f(x) = u_m(x) - \frac{1}{\beta_m^2}\frac{d^2 u_m(x)}{dx^2} \tag{7}$$

and its second order derivative

$$u_f''(x) = -\frac{d^2 u_m(x)}{dx^2} - \frac{1}{\beta_m^2}\frac{d^4 u_m(x)}{dx^4} \tag{8}$$

If Eq.8 is introduced in Eq.5b, the system in Eqs. 5 is replaced by a single fourth order differential equation

$$\frac{d^4 u_m(x)}{dx^4} + \frac{d^2 u_m(x)}{dx^2}\left(1 - \frac{\beta_f^2}{\beta_m^2}\right) = 0 \tag{9}$$

which represents the strong form of the equilibrium, ruling the axial behaviour of the the two trusses coupled by a continuous shear interface. It is observed that Eq.9 can be solved in $u_m(x)$, obtaining the field of axial elongations in the fabric from Eq.7. The solution of the homogeneous equation Eq.9 belongs to the following general form

$$u_m(x) = c_1\frac{e^{\eta x}}{\eta^2} + c_2\frac{e^{-\eta x}}{\eta^2} + c_3 x + c_4 \tag{10}$$

where

$$\eta = \sqrt{\beta_f^2 + \beta_m^2} \tag{11}$$

It should be noted that when the interface is infinitely deformable (i.e. $k = 0$), Eqs.5 represent the classic form of the equilibrium of two unloaded truss elements and Eq.10 describes the linear trend of the elongations.

Boundary conditions (BC) are enforced for particularizing Eq.10 and obtaining the solution of the scheme of Figure 1. In particular, compatibility conditions (essential BC) along the symmetry axis ($x = 0$) are enforced by considering that elongations are equal to zero

$$u_m(0) = 0 \tag{12a}$$

$$u_f(0) = \frac{d^2 u_m(x)}{dx^2}\Big|_{x=0} = 0 \tag{12b}$$

Additionally, equilibrium conditions need to be imposed at the ends of the two trusses. Reminding that the axial force inside the crack ($x = l$) is carried only by the fabric, the equilibrium conditions (natural BC) are written as follow

$$N_m(l) = \frac{du_m(x)}{dx}\Big|_{x=l} = 0 \tag{13a}$$

$$N_f(l) = \frac{du_f(x)}{dx}\Big|_{x=l} \frac{kt_i}{\beta_f^2} = F \tag{13b}$$

being F the overall axial force inside the crack sustained by the fabric.

The solution achieved in this way is expressed by the following function

$$u_m(x) = F\frac{e^{-\eta x}\beta_f^2\beta_m^2(e^{\eta l} - e^{\eta(l+2x)} + \eta x(e^{\eta x} + e^{\eta(2l+x)}))}{(1 + 2e^{2\eta l})kt_i\eta^3} \tag{14}$$

Eqs.14 and 7 represent the solution of the system. It should be noted that as expected the response of each component is linearly dependent from the value of applied force in the fabric and consequently, the functions $u_m(x)$ and $u_f(x)$ can be normalised with respect to F and adopted as general solutions for any value of force.

Finally, the trend of the axial force in the two trusses is found through the first order derivative of the axial elongations. In particular,

$$N_m(x) = \frac{kt_i}{\beta_m^2}\frac{du_m(x)}{dx} \tag{15a}$$

$$N_f(x) = \frac{kt_i}{\beta_f^2}\frac{du_f(x)}{dx} \tag{15b}$$

If Eq.14 and 7 are introduced in Eq.15, the following expressions hold

$$N_m(x) = F\beta_f^2\frac{e^{-\eta x}(e^{\eta x} - e^{\eta l} + e^{\eta(2l+x)} - e^{\eta(2l+x)})}{\eta^2(1+e^{2\eta l})} \tag{16a}$$

$$N_f(x) = F\frac{e^{-\eta x}(\beta_f^2 e^{\eta l} + \beta_f^2 e^{\eta(2x+l)} + \beta_m^2 e^{\eta x} + \beta_m^2 e^{\eta(2l+x)})}{\eta^2(1+e^{2\eta l})} \tag{16b}$$

It is observed that the fields of the axial force $N_m(x)$ and $N_f(x)$ are only a function of the relative stiffness parameters β_f, β_m and of the half crack spacing l, being linearly dependent from the F.

2.1. Numerical applications

Fig.3 shows the results of a numerical example, referring to an FRCM strip with $\beta_m = 0.01$, $\beta_f = 0.032$ and $s = 2l = 200mm$. Results are reported in normalised form with respect to F. The theoretical prediction of local effects in mortar and fabric layers seems to be in good agreement with experimental evidences, as can be observed in the study proposed by Saidi et Gabor [24]. It is observed as the trend of the axial elongations is more marked in the fabric with respect to the mortar. The trend of axial elongation in the fiber is almost linear in the central part of the specimen and tends to an exponential amplification near the loaded ends. Conversely, the slope of the axial elongation in the matrix assumes a constant value near the extremities of the strip. Fig.3(b) shows the trend of the normalised shear stress at the interface. It is observed that this trend reflects that

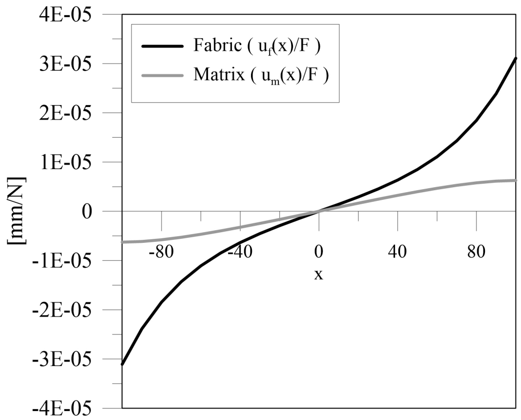

(a) Normalised axial elongations

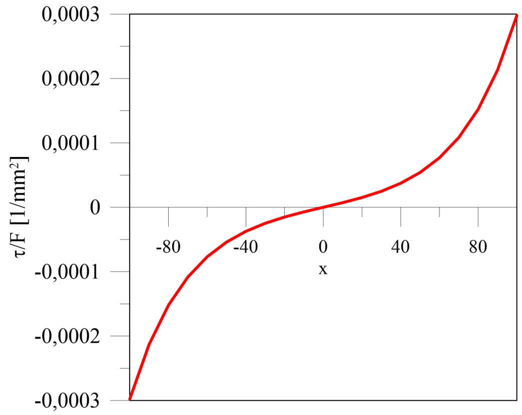

(b) Normalised shear stress

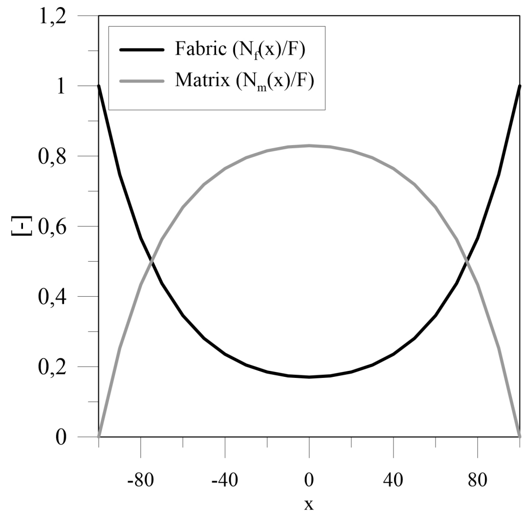

(c) Axial force

Figure 3: Numerical example for $\beta_m = 0.01$, $\beta_f = 0.032$, $s = 2l = 200mm$.

of the relative slip, calculated as $u_f(x) - u_m(x)$, multiplied for a magnification factor (i.e. the shear stiffness of the interface k). The shear stress tends to intensify at the ends of the element, near the cracks, due to the high value of the axial force sustained by the fiber in that zones. Finally, Fig.3(c) shows the trend of the normalised axial force in the two elements. It is observed as the axial load F entirely carried by the fabric for $x = l$

steeply decreases along the fiber down to its minimum value in correspondence of $x = 0$. Conversely, the axial force in the matrix $N_m(x)$ tends to increase from the crack $x = l$ to the middle section $x = 0$. It is observed that in this section the matrix carries a value of axial load equal to about the 40% of F. This trend of the axial force shows that the two elements interact through the interface and the transition of the axial stress from the fiber to the matrix is related to the shear stiffness of the interface k.

This mechanism is clear by comparing the results of Fig.3 with those reported in Fig.4. This last refers to an element with $\beta_m = 0.0045$, $\beta_f = 0.013$ and the same crack spacing of the previous example. It is observed that these lower values of β_m and β_f are obtained by adopting lower values of interface stiffness k. Results confirm that the contribution of the mortar becomes less evident for a more deformable interface (Fig.4(a)). The elongations in the matrix assume low values with respect to those in the fabric, and the trend of these last tends to be linear for lower value of k. As a consequence, the shear stresses are reduced with respect to the previous example, due to the increased deformability of the interface (Fig.4(b)). The trend of the shear stress almost reproduces that of the displacements in the fabric, and the interface is more uniformly stressed along its length with lower value of stresses. This fact is reflected in terms of axial force, as shown in Fig.4(c). As expected, the contribution of the matrix is less evident in this case. The values of axial force in the mortar are lower with respect to the previous case, due to the lower ability of the interface in transferring the stress from the loaded element to the matrix.

The effect of the interface stiffness on the force transmission of the element can be observed in Fig.5, which shows the normalised interface shear stress and the axial force in the fabric for different values of k, from 2 to 12 N/mm^3. It is worth noting that the shear stress keeps a similar trend in the central zone of the strip for the different values of k. When k increases, the slope of the function tends to rise suddenly and the response proves to be less sensitive to the value of the interface stiffness, as shown from the curves which

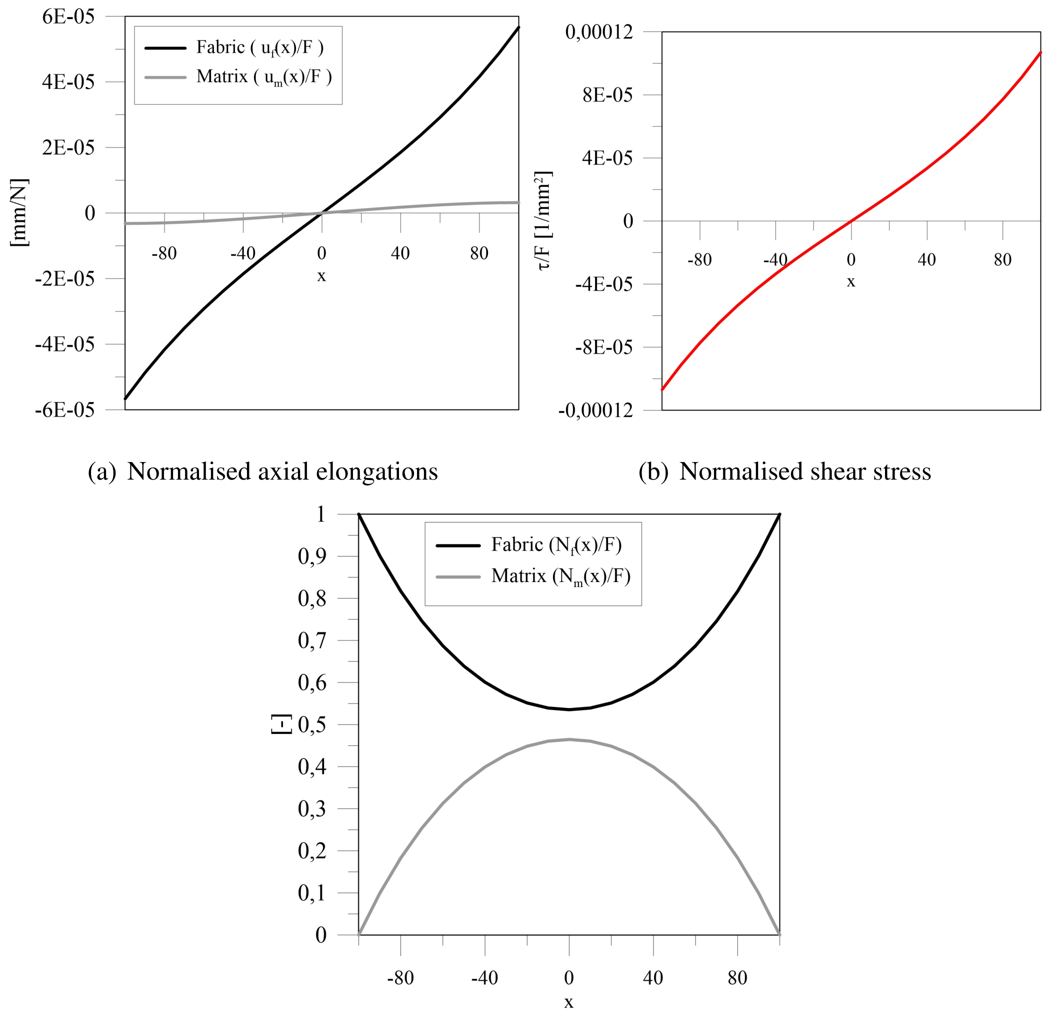

(a) Normalised axial elongations

(b) Normalised shear stress

(c) Axial force

Figure 4: Numerical example for $\beta_m = 0.0045$, $\beta_f = 0.013$, $s = 2l = 200mm$.

tend to be closer.

3. Model implementation

The proposed formulation of the coupled truss element can be exploited for calculating the constitutive tensile response of FRCM strips.

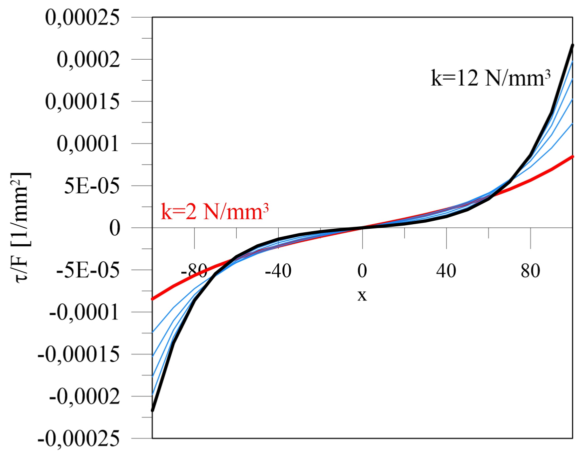

(a) Normalised shear stress

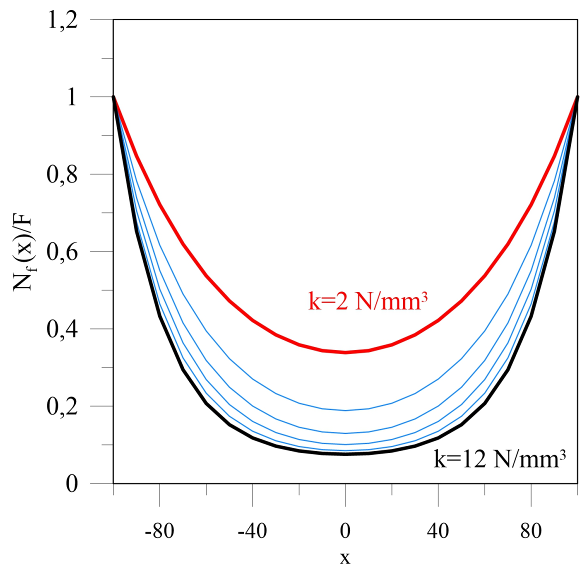

(b) Normalised axial force in the fabric

Figure 5: Parametric example for different values of k.

On the basis of the results presented in the previous section, it is possible to calculate the tensile load F_{cr} corresponding to the formation of a crack in correspondence of $x = 0$. In particular, the maximum axial stress in the matrix $N_m(0)/A_m$ can be imposed to be equal to the tensile strength of the mortar f_{mt}. The following relation holds

$$N_m(0) = f_{mt} t_i \frac{k}{E_m \beta_m^2} = \epsilon_{mt} \frac{k t_i}{\beta_m^2} = F_{mt} \tag{17}$$

being ϵ_{mt} the ultimate tensile strain of the matrix, and labelling F_{mt} the axial tensile capacity of the matrix within the strip.

If $N_m(0)$ is evaluated through Eq.16a for $x = 0$, Eq.17 can be considered an equation with a single unknown variable F_{cr}, which solution is represented by the following expression:

$$\frac{F_{cr}}{F_{mt}} = \frac{(e^{2\eta l} + 1)\eta^2}{(e^{\eta l} - 1)^2 \beta_f^2} \tag{18}$$

Finally, the stiffness of the system is obtained by dividing the value of F_{cr} for the value of $u_f(x)$ calculated for $x = l$ and for $F = F_{cr}$.

$$\frac{K_{cr}}{E_f A_f} = \frac{\eta^3 Cosh(\eta l)}{\eta l \beta_m^2 Cosh(\eta l) + \beta_f^4 Sinh(\eta l)} \tag{19}$$

Eq.19 represents the normalised axial stiffness of the coupled truss element considering the interaction between matrix and fabric. It is observed that both normalised expressions 18 and 19 depend only by the relative stiffness parameters β_f and β_m and from the half crack spacing l.

On the basis of the previous expressions, an easy procedure can be followed to calculate the axial force vs. displacement response of a FRCM strip. The procedure is based on the progressive assumption of the crack spacing s and number of cracks n_c, hypothesizing that the strip can be modeled by n_e series trusses (Fig.6).

The procedure can be resumed with the following points:

- the crack spacing at the first step s^I is assumed to be equal to the length of the strip L -i.e. two cracks are formed at the ends ($n_c^I = 2$)-;

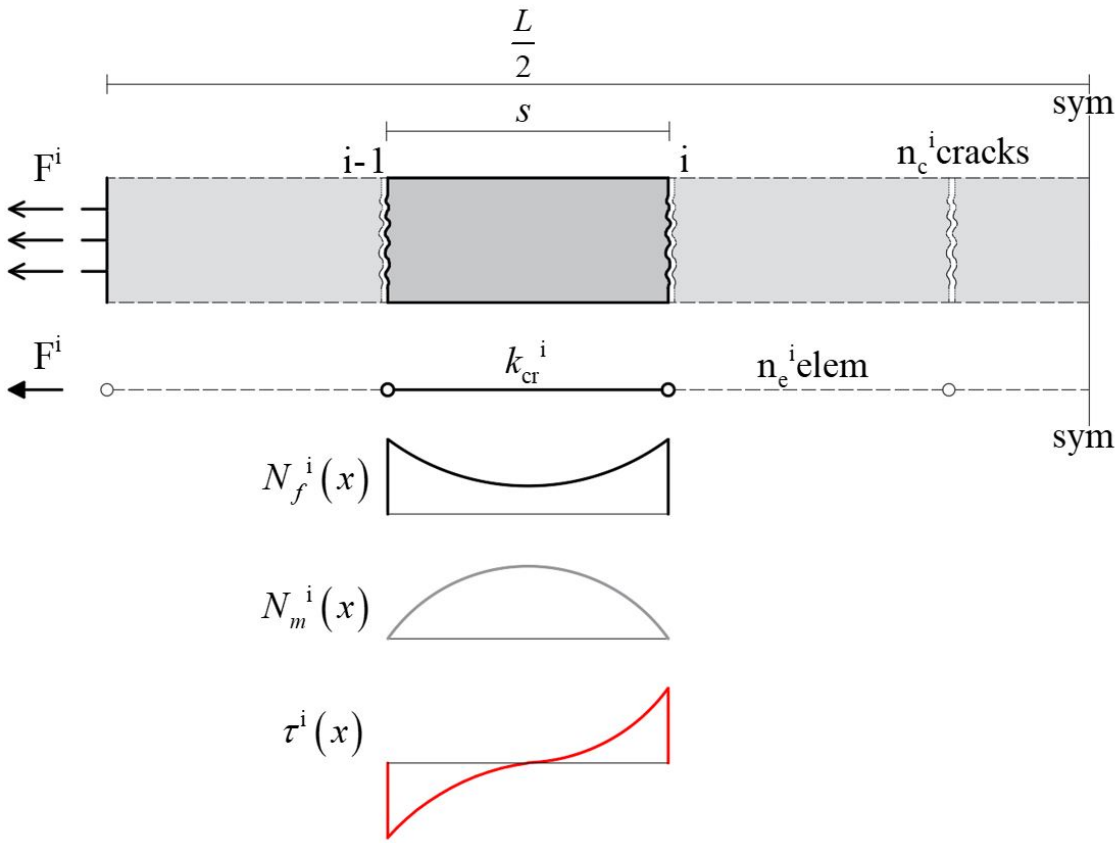

Figure 6: Series truss model

- the system is therefore made by $n_e^I = n_c^I - 1 = 1$ truss with stiffness equal to $K^I = K_{cr}$ evaluated through Eq.19;
- the force carried by the system F^I is calculated through Eq.18, assuming that a new crack is opened for $x = 0$;
- the elongation is therefore easily calculated $u^I = F^I/K^I$;
- the procedure is repeated from the first point, and for the general i-th step the following expressions can be considered:

$$n_e^i = 2^{(i-1)} \tag{20a}$$

$$n_c^i = n_e^i + 1 \tag{20b}$$

$$s^i = L/n_e^i \tag{20c}$$

$$\frac{1}{K^i} = \frac{n_e^i}{K_{cr}} \tag{20d}$$

- the procedure is interrupted when the force F^i exceeds the tensile strength of the textile or when the shear stress τ^i is greater than the maximum value assumed at the interface.

The use of Eq.20 together with the generalized expressions of the force Eq.18 and stiffness Eq.19 allows to evaluate the post-cracking tensile response of FRCM strips and to assess the number of cracks at failure.

Fig.7 shows two examples of application of the proposed model for a strip length of $L = 200$ mm, considering the two cases mentioned above of stiff (Fig.7(a)) and deformable interface (Fig.7(b)). The response is reported in terms of normalised axial force F/F_{mt} as per Eq.18, while the axial elongation is normalised with respect to the ultimate displacement of the mortar $\epsilon_{mt}L$. This kind of representation is due to the fact that it depends only by the parameters β_f, β_m and by the length of the strip L. The first point of the curve corresponding to the formation of the first crack is calculated by the well known expressions

$$F_{1stcr} = f_{mt}\left(A_m + \frac{E_f}{E_m}A_f\right) \tag{21a}$$

$$u_{1stcr} = \frac{F_{1stcr}}{E_m A_m + E_f A_f}L \tag{21b}$$

It is clear to observe that the behaviour of the two samples is completely different. The example with stiff interface (Fig.7(a)) shows a progressive hardening response, due

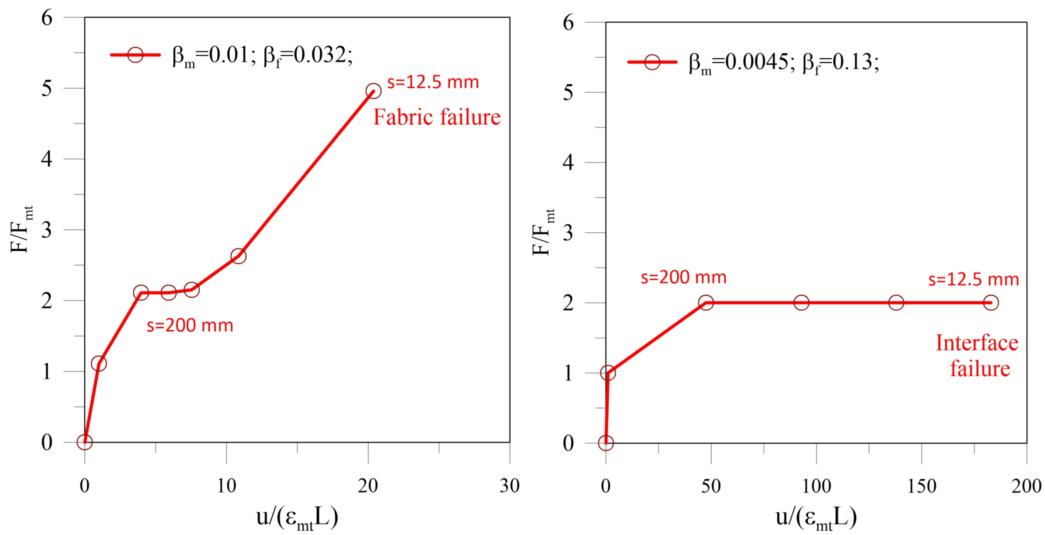

(a) $\beta_m = 0.01$, $\beta_f = 0.032$ (b) $\beta_m = 0.0045$, $\beta_f = 0.013$

Figure 7: Normalised axial load vs. normalised elongation response L=200 mm

to the stiffening behaviour provided by the mortar. In this case, as the number of cracks increases, the system tends to become stiffer. The axial load increases up to the maximum tensile capacity of the fabric. Differently, the example with deformable interface (Fig.7(b)) shows a limited tensile capacity, due to the fact that the contribution of the matrix can be considered negligible. Consequently, the system tends to face larger displacements with negligible contribution in terms of force and failure is reached due to the excessive slip between fabric and matrix.

3.1. Calibration of the interface stiffness

As discussed in the previous section, the representation of the tensile constitutive behaviour in dimensionless form is dependent only by the numerical parameters β_f and β_m. However, a reliable calculation of the tensile load vs. elongation curve needs a calibration of the dimensional parameters needed for calculating β_f and β_m - i.e. A_f, A_m and k.

In the current study, the area of the transverse cross section of the fabric A_f is assumed to be equal to the conventional equivalent area of a lamina of dry textile. This assumption, despite simplified, is coherent with the common conventional models adopted in the technical codes, especially for FRP composites. It is also observed that this assumption is an approximation of the area of the yarns, which makes possible to calculate the area of the fabric based on dimensional parameters. Coherently with this hypothesis, the thickness of the interface t_i is assumed equal to twice the width of the sample.

Finally, the model requires the definition of the interface stiffness k. It should be noted that this parameter can be considered as a function of the nature of the fiber and of the matrix. In fact, in general, the stiffness of a zero-thickness interface between two layers can be assessed as

$$k = \frac{G}{t_p} \tag{22}$$

being G the lower shear modulus of the two layers and t_p is the thickness of the process zone of the interface. In the context of the tensile behaviour of FRCM strips, the process zone of the interface can be considered equal to the cortical thickness of yarns embedded by the matrix. Obviously, t_p can be considered a function of the type of fiber and of its external treatment (coated or uncoated). For this reason, the parameter k is here calibrated as a function of the mechanical ratio of fabric ω, defined as

$$\omega = \frac{A_f f_t}{A_m f_{mt}} \tag{23}$$

being f_t the tensile strength of the fabric.

This parameter includes indirectly the shear deformability of the matrix through its tensile strength f_{mt} and the number of layers through the value of A_f. The value of the interface stiffness is therefore calibrated experimentally by evaluating the trend of k as a function of ω for different types of fiber. In particular, for each experimental data the value of k was evaluated as the optimal value which minimizes the difference between the experimental $E_{cr,exp}$ and the theoretical $E_{cr,th}$ value of dissipated energy during the post-cracking stage, this last calculated as the area under the tensile force vs. elongation response after first cracking. Table 1 shows the overall experimental database adopted

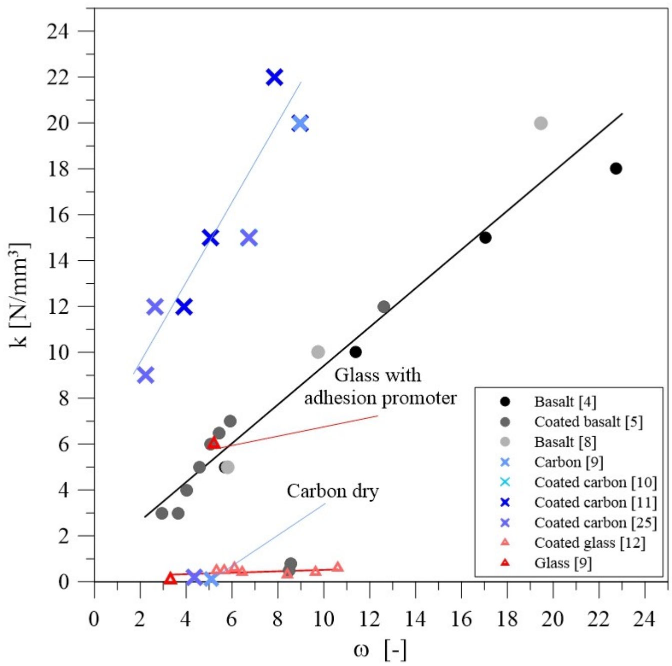

Figure 8: Calibration of k as a function of ω

for calibrating the value of k. The database includes the mechanical properties of fiber, matrix and the corresponding values of ω. The result of the calibration is shown in terms of ratio $E_{cr,exp}/E_{cr,th}$, and the resulting value of k. Basalt, carbon and glass FRCM were considered with different yarn treatment and for a wide range of ω. It is worth noting that PBO FRCM was not included in this database due to the different behaviour with the other types of fibres.

Fig.8 shows the results of the correlation between k and ω for all the considered data, grouped for kind of fibers and referring literature work. The graph shows that all the sets of experimental data can be fitted with good accuracy by a linear regression model, which equation depends on the kind of fiber. The application of the least squares approximation of the trend leads to the following results

$$k = 1.743\omega + 6.098 \text{ for coated carbon} \tag{24a}$$

$$k = 0.827\omega + 1.251 \text{ for basalt} \tag{24b}$$

$$k = 0.048\omega - 0.057 \text{ for glass} \tag{24c}$$

The reliability of these best fitting curves is confirmed by the values of the coefficient of determination R^2 reported in Fig.8. Values over 90% are obtained for all the cases, confirming that ω can be considered the independent variable for the calculation of k and given kind of fiber. It is observed that only two results were in contrast with the linear trend, as highlighted in the graph due to the application of a treatment on the yarns. Eq.24 are therefore valid only for coated carbon and fibers without adhesion promoter at the interface. Further experimental studies need to be addressed for verifying the application of a linear regression model on these systems.

4. Comparison with experimental results

The model was validated against the experimental results shown in Table 1. In the following only some examples are shown in graphical form for the sake of brevity.

Fig.9 shows the comparison between experimental data and theoretical predictions for basalt FRCM specimens with the experimental data achieved by Larrinaga et al. [4] and D'Anna et al. [8]. It is clear to observe that good agreement is generally obtained between predictions and experimental results. The model is able to consider the effect of the number of layers and it tends to slightly underestimate the response for the data of D'Anna et al. [8] especially for greater number of layers, while a negligible overestimation is observed for low number of layers for the data of [4]. It is also worth observing that

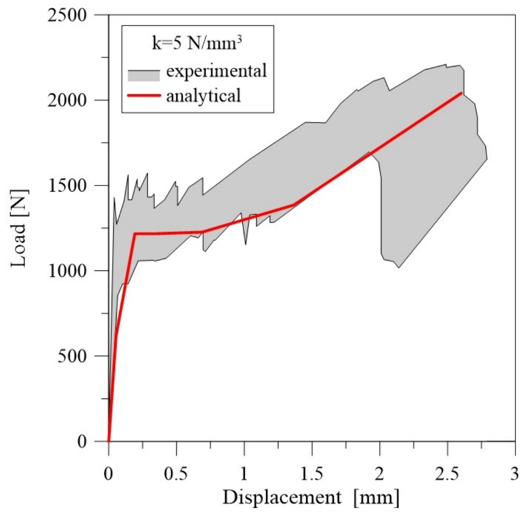

(a) One layer [8]

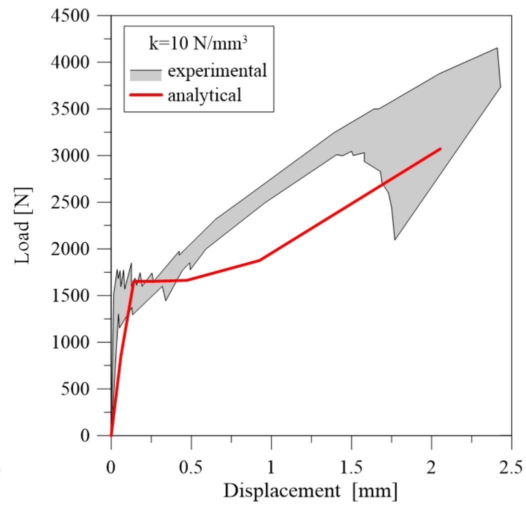

(b) Two layers [8]

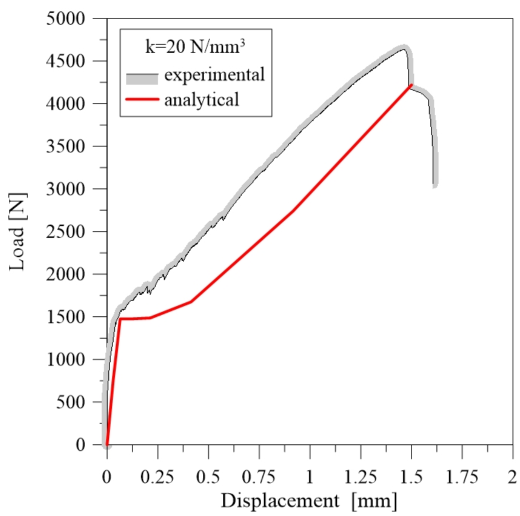

(c) Three layers [8]

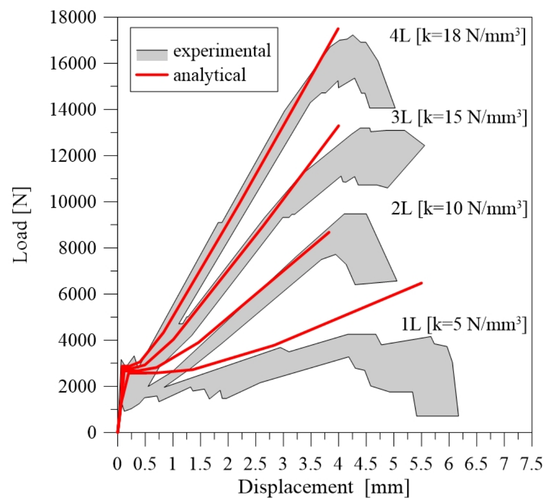

(d) Data of [4]

Figure 9: Comparisons with experimental data for basalt FRCM

for specimens tested by D'Anna et al. [8] the model provides an estimated step of cracks equal to about 31 mm, 25 mm and 19 mm for one, two and three layers respectively, while the experimental values of cracks spacing are 37 mm, 16 mm, and 11 mm for one, two and three layers respectively.

Similarly Fig.10 shows the comparison between predictions and experimental data available in the literature [9][10][11] for carbon FRCM specimens. Also in these cases the proposed procedure is capable of catching the average experimental response for different number of layers and for different sources of the experimental data. It is also worth observing that as expected the value of k increases for greater number of layers. Fig.11 shows similar comparisons for Glass FRCM specimens. Experimental data refer to the works of Bellini et al. [9], Bramato et al. [12] and Donnini et al. [26] . It is observed that lower values of k are associated to the tensile behaviour of the specimens, which usually shows a bilinear response with a negligible second stage. The model overestimates the first branch of the response for the cases of Fig.11(a) and 11(b), probably due to the uncertainties about the mechanical properties of the constituent materials, but fits well the experimental response in the last stage for all the data.

Tensile behaviour requires to take into account complex mechanisms. However, the proposed simplified theoretical model is able to simulate fairly well the behaviour of FRCM composites. It should be observed that the same experimental data were used for the calibration of k and therefore a more reliable validation should be made with new experimental results outside from the considered database.

5. Conclusions

This paper presented the proposal of a truss element for modelling the tensile response of FRCM strips. The model was formulated by studying the mechanics of force transmission between fabric and matrix within the crack spacing, assuming that the two phases

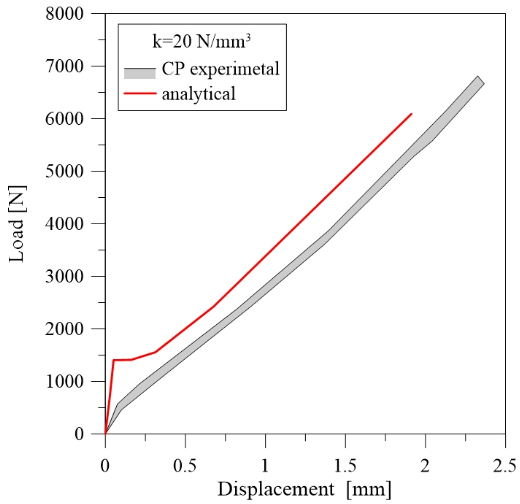

(a) Data of [9] carbon fibers with adhesion promoter

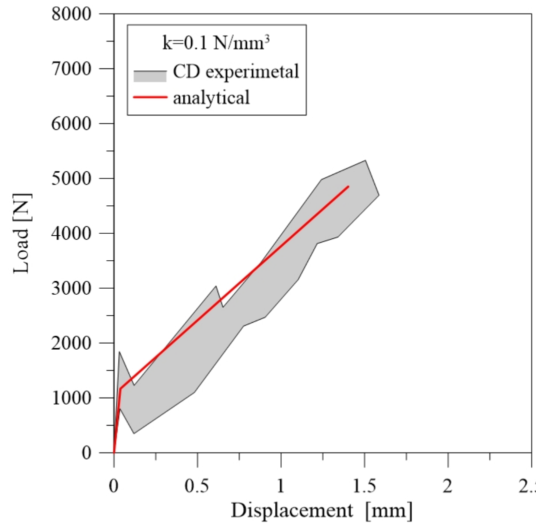

(b) Data of [9] dry carbon

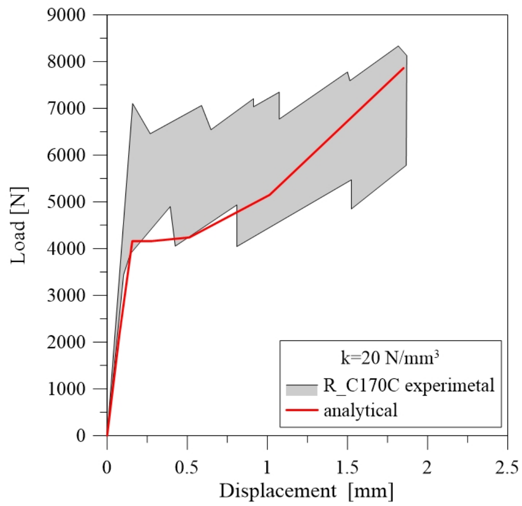

(c) Data of [10] coated carbon

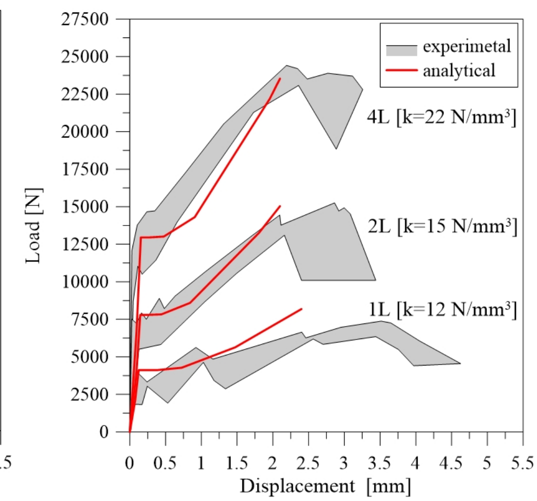

(d) Data of [11] coated carbon

Figure 10: Comparisons with experimental data for Carbon FRCM

can be studied as truss elements connected through a shear interface. The definition of the coupled truss allows to set a procedure for obtaining the tensile response of the composite material, under the assumption of linear behaviour of fabric, matrix and interface.

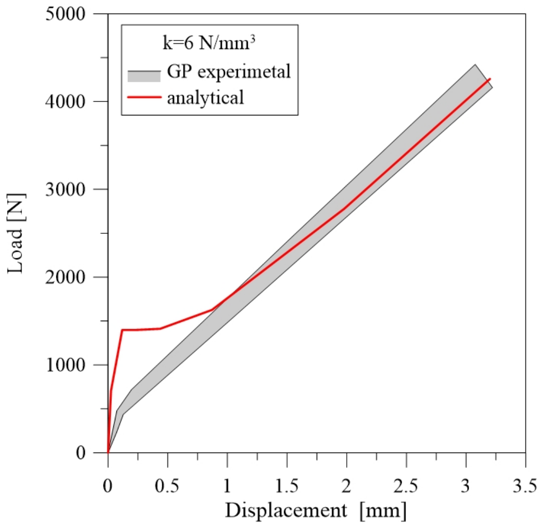

(a) Data of [9] glass fibers with adhesion promoter

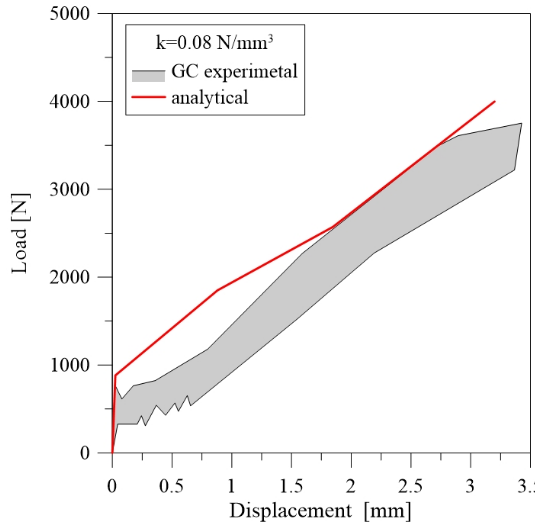

(b) Data of [9] coated glass fibers

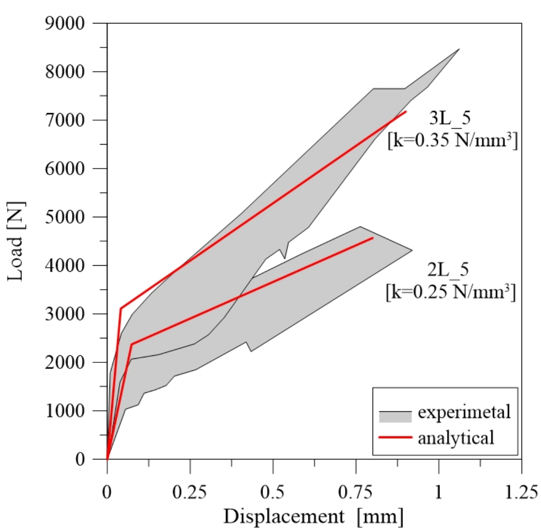

(c) Data of [12] coated glass fibers

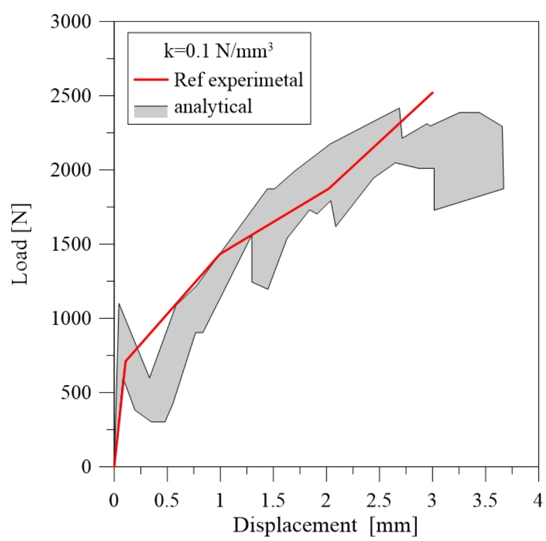

(d) Data of [26] coated glass fibers

Figure 11: Comparisons with experimental data for Glass FRCM

On the basis of the obtained results and for the range of analyzed variables, the following conclusions can be drawn:

- the numerical parameters β_m and β_f rule the force transmission mechanism between matrix and fabric. Force in the fabric and interface shear stress tend to intensify in correspondence of the cracks for greater values of k (i.e. stiffer interface);

- the normalised representation of the tensile response of FRCM strips F/F_{mt} vs. $u/(\epsilon_{mt}L)$ proved to be dependent only by the numerical parameters β_m, β_f and from the length of the strip L;

- it should be considered that previous studies showed that the form of textile reinforcement cross-section has a substantial influence on the load carrying capacity of FRCM. However the parameter k can be considered a function of the mechanical ratio of fabric reinforcement ω and from the nature of the fiber. The experimental calibration of k allows to find a linear variation of k as a function of ω for different kinds of fiber. However, this correlation proved to be affected by the treatment of the yarns and different results can be achieved for fibers applied with adhesion promoter;

- the proposed procedure was validated against experimental results available in the literature, proving to be reliable. It should be noted that the validation was made against experimental data included in the database for the calibration of k and for this reason, further experimental investigation should be made for a broader validation of the model.

Acknowledgements

This research was supported by a grant from the Italian Ministry for University and Research (MIUR) for PRIN-2017 project "Innovative systems based on inorganic mortar and non metallic reinforcement for the upgrade of masonry structures and non structural elements". The financial support is gratefully acknowledged.

This research was developed among the activity of the Project ReLUIS "Progetto Esecutivo Accordo DPC/ReLUIS 2019-2021, WP14 - Contributi normativi per Materiali Innovativi per Interventi su Costruzioni Esistenti".

References

[1] G. Amato, J. Chen, J. D'Anna, L. La Mendola, G. Minafò, FRCM systems for strengthening masonry structures, Advanced Composites in Construction, ACIC 2017 - Proceedings of the 8th Biennial Conference on Advanced Composites in Construction (2017) 244–249.

[2] A. Bilotta, F. Ceroni, E. Nigro, M. Pecce, Experimental tests on FRCM strengthening systems for tuff masonry elements, Construction and building Materials 138 (2017) 114–133.

[3] J. Donnini, V. Corinaldesi, Mechanical characterization of different FRCM systems for structural reinforcement, Construction and Building Materials 145 (2017) 565–575.

[4] P. Larrinaga, C. Chastre, H. C. Biscaia, J. T. San-José, Experimental and numerical modeling of basalt textile reinforced mortar behavior under uniaxial tensile stress, Materials & Design 55 (2014) 66–74.

[5] G. P. Lignola, C. Caggegi, F. Ceroni, S. De Santis, P. Krajewski, P. B. Lourenço, M. Morganti, C. C. Papanicolaou, C. Pellegrino, A. Prota, et al., Performance assessment of basalt FRCM for retrofit applications on masonry, Composites Part B: Engineering 128 (2017) 1–18.

[6] C. Caggegi, E. Lanoye, K. Djama, A. Bassil, A. Gabor, Tensile behaviour of a

basalt TRM strengthening system: Influence of mortar and reinforcing textile ratios, Composites Part B: Engineering 130 (2017) 90–102.

[7] J. D'Anna, G. Amato, J. F. Chen, G. Minafò, L. La Mendola, Experimental investigation on basalt grid cementitious mortar strips in tension, in: Civil Engineering Research in Ireland 2018-CERI 2018, IE, 2018.

[8] J. D'Anna, G. Amato, J. F. Chen, G. Minafò, L. La Mendola, On the use of digital image correlation (DIC) for evaluating the tensile behaviour of BFRCM strips, in: Key Engineering Materials, volume 817, Trans Tech Publ, 2019, pp. 377–384.

[9] A. Bellini, M. Bovo, C. Mazzotti, Experimental and numerical evaluation of fiber-matrix interface behaviour of different FRCM systems, Composites Part B: Engineering 161 (2019) 411–426.

[10] T. D'Antino, C. C. Papanicolaou, Comparison between different tensile test set-ups for the mechanical characterization of inorganic-matrix composites, Construction and Building Materials 171 (2018) 140–151.

[11] L.-L. Wei, J.-H. Zhu, T. Ueda, M.-N. Su, J. Liu, W. Liu, L.-P. Tang, F. Xing, Tensile behaviour of carbon fabric reinforced cementitious matrix composites as both strengthening and anode materials, Composite Structures 234 (2020) 111675.

[12] G. Bramato, A. Cascardi, F. Micelli, M. A. Aiello, Tensile characterization of multi-ply fabric-reinforced cementitious matrix, in: 3rd RILEM Spring Convention, Guimaraes, RILEM, 2020.

[13] E. Bertolesi, F. Carozzi, G. Milani, C. Poggi, Numerical modeling of fabric reinforce cementitious matrix composites (FRCM) in tension, Construction and Building Materials 70 (2014) 531–548.

[14] C. Caggegi, F. G. Carozzi, S. De Santis, F. Fabbrocino, F. Focacci, Ł. Hojdys, E. Lanoye, L. Zuccarino, Experimental analysis on tensile and bond properties of PBO and aramid fabric reinforced cementitious matrix for strengthening masonry structures, Composites Part B: Engineering 127 (2017) 175–195.

[15] D. Arboleda, F. G. Carozzi, A. Nanni, C. Poggi, Testing procedures for the uniaxial tensile characterization of fabric-reinforced cementitious matrix composites, Journal of Composites for Construction 20 (2016) 04015063.

[16] S. De Santis, H. A. Hadad, F. De Caso y Basalo, G. De Felice, A. Nanni, Acceptance criteria for tensile characterization of fabric-reinforced cementitious matrix systems for concrete and masonry repair, Journal of Composites for Construction 22 (2018) 04018048.

[17] G. Minafò, L. La Mendola, Experimental investigation on the effect of mortar grade on the compressive behaviour of FRCM confined masonry columns, Composites Part B: Engineering 146 (2018) 1–12.

[18] A. Monaco, J. D'Anna, M. C. Oddo, G. Minafò, L. La Mendola, Numerical modelling of the tensile behaviour of BFRCM strips, in: Key Engineering Materials, volume 817, Trans Tech Publ, 2019, pp. 15–22.

[19] A. Monaco, G. Minafò, J. D'Anna, M. C. Oddo, L. La Mendola, Constitutive numerical model of FRCM strips under traction, Frontiers in Built Environment 6,60 (2020).

[20] E. Grande, G. Milani, Numerical simulation of the tensile behavior of FRCM strengthening systems, Composites Part B: Engineering (2020) 107886.

[21] G. Milani, E. Grande, Simple bisection procedure in quickly convergent explicit ODE solver to numerically analyze FRCM strengthening systems, Composites Part B: Engineering 199 (2020) 108322.

[22] M. Molter, Load-bearing capacity and serviceability of textile reinforced bending beams, Proceedings of First Colloquium on Special Research Areas 528 and 532 Aachen University (2001) 205–219.

[23] S. Ohno, D. J. Hannant, Modelling the stress-strain response of continuous fiber reinforced cement composites, ACI Materials Journal 91, No.3 (1994) 306–312.

[24] M. Saidi, A. Gabor, Experimental analysis of the tensile behaviour of textile reinforced cementitious matrix composites using distributed fibre optic sensing (dfos) technology, Construction and Building Materials 230 (2020) 117027.

[25] F. G. Carozzi, A. Bellini, T. D'Antino, G. de Felice, F. Focacci, Ł. Hojdys, L. Laghi, E. Lanoye, F. Micelli, M. Panizza, et al., Experimental investigation of tensile and bond properties of carbon-FRCM composites for strengthening masonry elements, Composites Part B: Engineering 128 (2017) 100–119.

[26] J. Donnini, F. Bompadre, V. Corinaldesi, Tensile behavior of a glass FRCM system after different environmental exposures, Processes 8 (2020) 1074.

Table 1: Experimental database

Ref.	**ID sample**	**Fiber Type**	$E_f[GPa]$	**Mortar Type**	$f_{mt}[MPa]$	**k** $[N/mm^3]$	$\frac{E_{cr,exp}}{E_{cr,th}}$	ω
[4]	TB1	Basalt	67	cement-based	2.48	5	1.06	5.7
	TB2	Basalt	67	cement-based	2.48	10	0.98	11.4
	TB3	Basalt	67	cement-based	2.48	15	0.99	17.1
	TB4	Basalt	67	cement-based	2.48	18	1.07	22.7
[5]	FRCM 1	Coated basalt	110	cement-based	0.80	0.8	0.85	8.6
	FRCM 1	Coated basalt	116	cement-based	1.50	4	1.09	4.0
	FRCM 1	Coated basalt	111.5	cement-based	1.30	6	0.99	5.1
	FRCM 2	Coated basalt	111.5	lime-based	1.20	6.5	1.16	5.4
	FRCM 2	Coated basalt	107	lime-based	1.00	12	1.03	12.6
	FRCM 3	Coated basalt	71.3	lime-based	1.30	7	1.12	5.9
	FRCM 4	Coated basalt	89	lime-based	0.50	0.5	0.97	8.5
	FRCM 4	Coated basalt	51	lime-based	0.50	3	1.06	3.0
	FRCM 4	Coated basalt	45.3	lime-based	1.00	3	0.96	3.7
	FRCM 4	Coated basalt	45.3	lime-based	0.80	3	1.07	4.6
[8]	1L	Basalt	83	cement-based	2.00	5	1.24	5.8
	2L	Basalt	83	cement-based	2.00	10	1.17	9.6
	3L	Basalt	83	cement-based	2.00	20	1.21	19.5
[9]	CP	Carbon$^{(*)}$	240	hydraulic lime-based	1.92	20	1.14	9.0
	CD	Carbon	240	hydraulic lime-based	2.91	0.1	1.36	5.1
	GP	Glass$^{(*)}$	65	hydraulic lime-based	1.92	6	0.94	5.2
	GC	Coated glass	70	hydraulic lime-based	2.00	0.08	0.88	3.3
[10]	R- C170CC	Coated carbon	219	cement-based	3.35	15	1.14	6.7
[11]	L1	Coated carbon	196.4	cement-based	2.50	12	0.79	3.91
	L2	Coated carbon	196.4	cement-based	2.50	15	0.96	5.1
	L4	Coated carbon	196.4	cement-based	2.50	22	1.01	7.8
[12]	1L	Coated glass	108	lime-based	1.00	0.3	1.19	10.6
	2L-3	Coated glass	108	lime-based	2.00	0.55	1.06	12.9
	3L-3	Coated glass	108	lime-based	2.20	0.55	1.05	13.2
	2L-5	Coated glass	108	lime-based	2.50	0.25	0.81	5.7
	3L-5	Coated glass	108	lime-based	2.50	0.35	0.93	6.9
	2L-10	Coated glass	108	lime-based	1.10	0.25	0.99	6.4
	3L-10	Coated glass	108	lime-based	1.50	0.3	0.96	5.3
[25]	FRCM 6	Coated carbon	187	cement-based	3.35	12	1.26	2.6
	FRCM 6	Coated carbon	219	cement-based	4.00	9	1.12	2.22
[26]	Ref	Coated glass	67.58	cement-based	0.80	0.1	0.84	4.3
	S-40	Coated glass	67.87	cement-based	0.80	0.1	0.90	4.0
	A-40	Coated glass	69.37	cement-based	0.90	0.08	0.87	2.9
	FT	Coated glass	66.21	cement-based	0.80	0.09	0.86	4.0

$^{(*)}$ Adhesion promoter